ELSEVIER

Journal of Nuclear Materials 276 (2000) 269–277

journal of nuclear materials

www.elsevier.nl/locate/jnucmat

Study of defect annealing behaviour in neutron irradiated Cu and Fe using positron annihilation and electrical conductivity

M. Eldrup*, B.N. Singh

Materials Research Department, Risø National Laboratory, DK-4000 Roskilde, Denmark

Abstract

To compare the defect accumulation and the annealing behaviour in an fcc and a bcc metal, OFHC-Cu and pure Fe were neutron irradiated at 100°C to a fluence of 1.5×10^{24} n/m^2, ($E>1$ MeV). Isochronal annealing was carried out and the annealing behaviour followed by positron annihilation spectroscopy (PAS) as well as electrical conductivity measurements. The results for the two specimens in the as-irradiated state are very different. In Cu the defect positron lifetime is characteristic of single vacancies, very small vacancy clusters or stacking fault tetrahedra, while in Fe the defect lifetimes confirm the presence of micro-voids and voids. The electrical conductivity, on the other hand does not discriminate between the two types of damage in the irradiated specimens. During annealing of the irradiated Fe below stage V, the average void size grows by migration and coalescence of the micro-voids and voids. At and above stage V the void density decreases and the voids finally anneal out at ~500°C. In contrast, the annealing of irradiated Cu below stage V does not yield any evidence for the evolution of micro-voids or voids. The implications of these results are discussed. One conclusion is that neutron irradiation below stage V causes higher void swelling in bcc iron than in fcc copper.

PACS: 78.70.Bj; 71.60.+z; 61.80.-x; 61.80.Hg

1. Introduction

The problem of defect accumulation in the form of loops, tetrahedra and voids in irradiated metals has been studied both in fcc and bcc metals and alloys over a long period of time. Recently, Singh and Evans [1] have reviewed the available experimental results and have shown that there exist rather large differences in defect accumulation behaviour between fcc and bcc metals, particularly when irradiated under cascade damage conditions.

One of the significant differences in the defect accumulation behaviour between fcc and bcc metals is found to be in the area of void nucleation. Transmission electron microscopy (TEM) results clearly demonstrate, for example, that void nucleation in the studied bcc metals occurs already at temperatures just above the recovery stage III (see Table 2 in [1] and Fig. 1 in [2]) whereas in fcc metals voids have not been observed to nucleate much below the recovery stage V [1]. Singh and Evans [1] suggested that these differences in the nucleation behaviour of voids may, at least qualitatively, be rationalised in terms of a difference in the evolution of vacancy supersaturation during irradiation. The difference in supersaturation would be expected from the facts that (a) in bcc iron the intracascade clustering of vacancies (in the form of loops and/or stacking fault tetrahedra (SFT)) is considerably less efficient than that in fcc copper (see e.g. [3–6]) and (b) a higher fraction of self-interstitial atoms (SIAs) would be transported to sinks (e.g. dislocations and grain boundaries) via one-dimensional glide of small SIA clusters in bcc iron than in fcc copper (molecular dynamics calculations show that practically all SIA clusters in bcc iron are glissile [7,8]).

At present there is no proper theoretical model that gives a quantitative description of the above suggestion. Experimental data relating to this are therefore important, since they may prove useful in constructing a suitable theoretical framework to describe the energetics and kinetics of void nucleation in bcc and fcc metals and alloys. Relevant experimental information is also very

* Corresponding author. Tel.: +45-46 775 728; fax: +45-46 775 758.

E-mail address: morten.eldrup@risoe.dk (M. Eldrup)

0022-3115/00/$ - see front matter
PII: S0022-3115(99)00186-5

useful for comparison with Monte Carlo type simulations of damage accumulation under cascade damage conditions. The experimental data that have led to the suggestions outlined above have been obtained by TEM. However, the resolution of TEM puts a lower limit on the void sizes that can be observed. This may be the reason why in bcc Fe no voids have been detected after irradiation at low temperatures (i.e. at $\sim 0.2T_m$ where T_m is the melting point) [3,9]. Similarly, it is reasonable to ask if it is this limited TEM resolution which might have been the reason as to why no voids have been detected at low temperatures in fcc metals.

Based on such considerations and since positron annihilation spectroscopy (PAS) can detect the presence of single vacancies, vacancy clusters, voids and other vacancy type defects [10], it was decided to use this technique to study the nature and properties of the different kinds of vacancy agglomerates formed during neutron irradiation in an fcc and a bcc metal. Furthermore it was decided to investigate the defect evolution during post-irradiation isochronal annealing. In the present paper we report the results of this PAS study. The chosen metals were copper (fcc) and iron (bcc). The neutron irradiation was carried out at a temperature of 100°C. For both metals this temperature is above the annealing stage III and below stage V.

In the following section (Section 2) a brief outline of the basis of defect characterization by PAS is given. This is followed by details of materials and experimental procedures used in the present investigations (Section 3). The results of PAS and electrical conductivity measurements are described in Section 4. The physical meaning of the results and their implications regarding void nucleation are discussed in Section 5. The main conclusions, particularly related to the differences in the defect accumulation behaviour between bcc iron and fcc copper are presented in Section 6.

2. Characterization of defects and defect agglomerates by PAS

The physical basis for the use of positrons in defect studies is the fact that positrons injected into a material may get trapped at defects that represent regions where the atomic density is lower than the average density in the bulk, i.e vacancies, vacancy clusters (including voids and bubbles) and dislocations. Since positrons and electrons are antiparticles an injected positron will annihilate with an electron of the material. As a result, gamma-rays will be emitted. These γ-quanta carry information about the state of the positron before annihilation and by proper measurement of the emitted γ-quanta it is therefore possible to obtain useful information about those defects that have trapped the positrons. The experimental techniques used for these kinds of measurements are often referred to as 'positron annihilation spectroscopy' (PAS). In the present work the lifetimes of the injected positrons have been measured and so-called positron lifetime spectra have been obtained. Examples of such spectra are shown in Fig. 1.

Normally, regions of lower-than-average atomic density also have lower-than-average electron density. The lifetime of positrons trapped in defects will depend on the average electron density in the defects (the lower the electron density, the longer is the lifetime). So in principle, each type of defect gives rise to a characteristic positron lifetime, τ_i. If several types of defects are present in a sample this will therefore result in a lifetime spectrum for that sample which consists of several lifetime components. Each component is a decaying exponential, the slope of which equals the annihilation rate ($=\tau_i^{-1}$). Fig. 1 shows both single- and multi-component spectra. The purpose of the data analysis is to separate the various components and to determine their

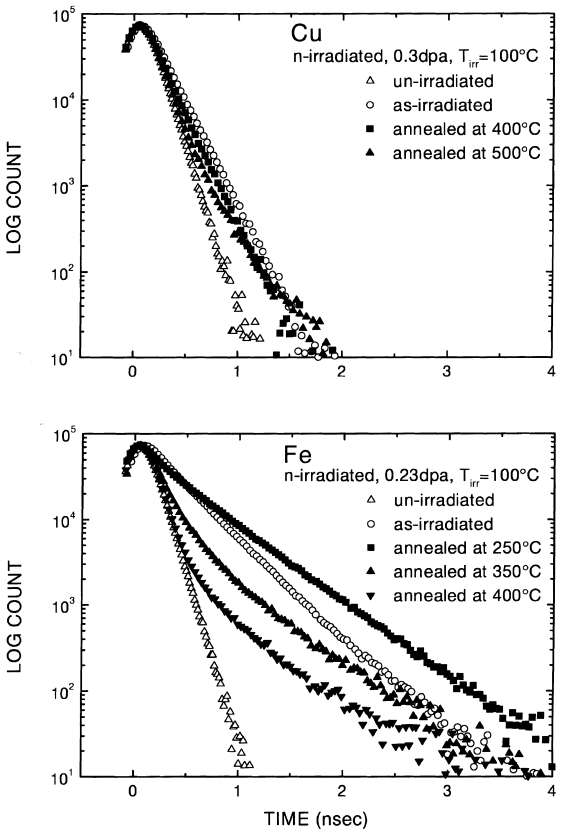

Fig. 1. Positron lifetime spectra for irradiated and annealed pure copper (top) and pure iron (bottom). Spectra for the unirradiated metals are also shown for comparison. The spectra for Fe clearly contain components with much longer lifetimes than the spectra for Cu. Such long lifetimes are indicative of the presence of micro-voids and voids.

lifetimes τ_i and intensities I_i (i.e. the relative areas under each component in a spectrum). Usually, the lifetimes are numbered from the shorter to the longer lifetimes (τ_1, τ_2, τ_3, etc.). The intensities are measures of the fractions of positrons that annihilate with the equivalent lifetimes. A certain lifetime value is then characteristic for positrons that annihilate either in the bulk material or trapped in a certain type of defects. In practice, it is possible to resolve only two or three lifetime components in a spectrum for a metal, so in some cases two or more components merge into one. A more detailed discussion of PAS can be found in e.g. [10,11] and references therein.

In bulk Cu and Fe the positron lifetime is 110 and 106 ps, respectively, while in defects such as monovacancies, dislocations, loops and SFTs the lifetimes are found to be in the range from ~120 to ~180 ps for both metals [10–19]. The lifetime of positrons trapped in three-dimensional vacancy agglomerates (voids) increases with the size of the voids up to a saturation value of about 500 ps for voids containing more than ~40–50 vacancies [10,16–18]. Thus, for small (sub-microscopic) voids the lifetime value is a measure of their size.

Positron annihilation spectroscopy has previously been applied in a number of studies of defect creation, interaction and recovery in metals and alloys. The sensitivity of PAS to vacancies and vacancy clusters has been used in many annealing experiments, for example to investigate the nature of the annealing stage III, in Cu [20,21], Ni [15], Fe [14,22,23], Mo [24,25] and a number of other metals [11]. The general picture is that the formation of vacancies (after low-energy electron irradiation) or small vacancy clusters (after high-energy electron, ion or neutron irradiation) is observed after irradiation below stage III. On annealing through stage III in most cases the migration and clustering of vacancies is evidenced by an increase of the positron lifetime [10]. It is interesting that for neutron irradiated Fe and Mo the lifetime increase begins appreciably below stage III. This has been interpreted as correlated clustering of subcascades into micro-voids [23,24,26]. There seems to be no PAS studies of fcc metals that have been neutron irradiated below stage III. However in Ni, irradiated with 28 MeV electrons [15] or 12.3 MeV protons [27], and in Al irradiated with 9.5 MeV electrons [28] there is no indication of a similar increase in lifetime below stage III that could indicate the formation of micro-voids.

3. Experimental procedure

The specimens used for the PAS and electrical conductivity measurements were standard tensile test specimens [29] of OFHC-Cu and Fe of 99.994 wt% purity. The sample thickness was about 0.3 mm for both metals. These specimens were neutron irradiated in the DR-3 reactor at Risø at 100°C to a fluence of 1.5×10^{24} n/m^2 ($E > 1$ MeV) equivalent to ~0.3 displacements per atom (NRT) (dpa) for Cu and ~0.23 dpa for Fe. For the electrical conductivity measurements the tensile specimens were used as described in [30]. For the PAS measurements, two samples of approximately 6×5 mm^2 were cut from one tensile specimen of each metal. Before isochronal annealing and PAS measurements were carried out, the sample surfaces were cleaned by chemical etching (Cu) or electro polishing (Fe).

Isochronal annealing of the specimens was made in vacuum ($\sim 2 \times 10^{-4}$ Pa) in steps of 50°C with a hold time of 50 min at each annealing step. Electrical conductivity measurements and PAS were done after each step.

The electrical conductivity measurements were carried out as described in [30]. For the PAS measurements a ^{22}Na positron source (encapsulated in two thin Ni foils) was placed between two samples of Cu or Fe. In a conventional positron lifetime spectrometer, two detectors are placed close to the source–sample sandwich to detect the emission (signalled by a 1.28 MeV γ-quantum) and the annihilation (signalled by a 511 keV γ-quantum) of the positrons, thus making it possible to obtain their lifetime, i.e. the time difference between the two signals. However, in the present measurements the samples themselves are radioactive. After neutron irradiation both metals contain various γ emitting isotopes, in particular ^{60}Co which emits a coincident pair of γ-rays. They give rise to an additional component in the measured lifetime spectra, if a standard lifetime spectrometer is used. In order to avoid this complication, we have added a third detector to the spectrometer. When a positron annihilates, normally two γ-quanta of 511 keV each are emitted in opposite directions. Thus, by putting two detectors opposite to each other that detect these two annihilation quanta in coincidence it is possible to select those events that originate from positrons and suppress those events which do not. This principle is described in some detail in [31].

In the present measurements a positron source of an activity of ~1 MBq was used. The irradiated Cu and Fe specimens had activities that were about the same as the source and 10 times higher, respectively. In a conventional two-detector spectrometer this gave rise to a count rate in the lifetime spectrum of ~120 counts/s. Of these, about 11% (Cu) or 17% (Fe) were due to the sample activity and would have to be corrected for, a correction that is not straightforward. Application of the new three-detector spectrometer reduces the count rate from the positrons by a factor of about 5, but the count rate from the sample activity was reduced by a factor of ~30 (Cu) or ~65 (Fe). The contribution to a lifetime spectrum from the sample activity is therefore reduced to roughly 2%, a correction which poses no problem.

The measured lifetime spectra contained a total of 1×10^6–3×10^6 counts. At several annealing temperatures spectra were measured more than once to assure reproducibility. Parallel with the measurements on the irradiated Cu and Fe, reference spectra for well-annealed Cu were recorded under the same conditions, i.e. with the sample in the same position, with the same positron source, and with a piece of irradiated Cu or Fe put close to the detectors to secure the proper count rates in the detectors.

The measured lifetime spectra were analysed with the PATFIT programs [32]. The reference spectra were used to determine the time resolution of the spectrometer and the correction for positrons annihilating in the source. Small variations of the time resolution during the measuring period were taken into account in the analysis of the spectra for irradiated Cu and Fe.

4. Results

To illustrate directly the obtained positron lifetime data, some of the lifetime spectra are shown in Fig. 1. Clearly, the spectra for Cu and Fe are qualitatively different: The lifetimes are appreciably longer for Fe than for Cu.

The quantitative analysis by POSITRONFIT [32] showed that the Cu spectra could be resolved into two components. The two lifetimes and the intensity of the long-lived component as functions of annealing temperature are shown in Fig. 2.

The spectra for irradiated and annealed Fe could be resolved into three lifetime components at all annealing temperatures. At the temperatures (250–350°C) where the longest lifetime, τ_3, is most well-defined, it scatters only a few ps around ~500 ps. At lower and higher temperatures the scatter is larger, but the average value is 502 ps. This lifetime is in the range of lifetimes expected for large (>40–50 vacancies) three-dimensional vacancy agglomerates (i.e. voids). We have therefore made the reasonable assumption that $\tau_3 = 502$ ps in the whole temperature range. In order to reduce the scatter on the other lifetimes and intensities we fixed $\tau_3 = 502$ ps in the final analysis of the data. The resulting parameters are shown in Fig. 3.

The trapping of positrons into one type of defects takes place in competition with trapping into other types of defects and with annihilation in the bulk. This competition has been modelled by simple rate equations, often referred to as the 'trapping model' [10]. The model is based on the assumption that there are one or more types of (homogeneously distributed) defects that trap the positrons. As mentioned above, each type of defect gives rise to a characteristic lifetime ($\tau_2, \tau_3, \ldots$) in a measured lifetime spectrum. The intensity of each lifetime component ($I_2, I_3, \ldots$) contains information about

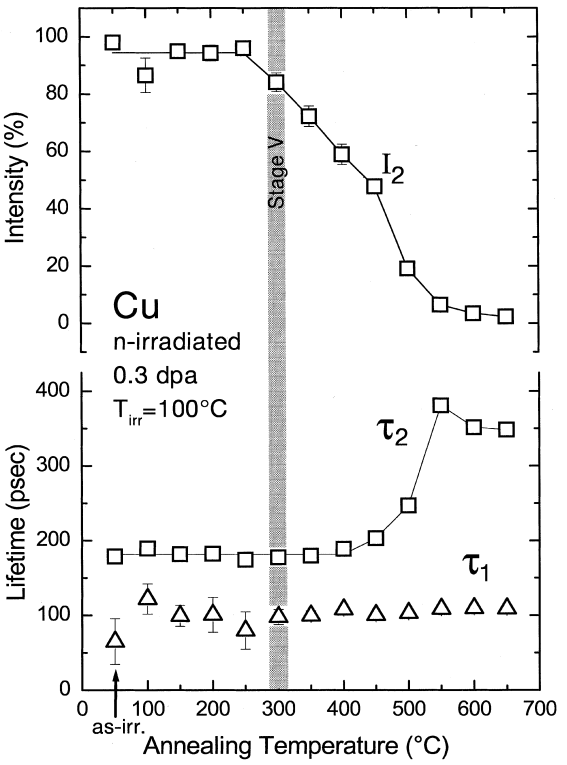

Fig. 2. The two positron lifetimes and the intensity of the long-lived component ($I_1 + I_2 = 100\%$) extracted from the spectra for the neutron irradiated Cu as functions of post-irradiation annealing temperature. The shaded band indicates the temperature of the recovery stage V. Some of the error bars are smaller than the sizes of the data point symbols and have therefore not been shown.

the fraction of positrons that are trapped in the particular type of defect. By inserting the measured values of intensities and lifetimes (Figs. 2 and 3) into the trapping model it is possible to derive the rates with which positrons are trapped into the defects. The trapping rates calculated from the Cu and Fe data are shown in Figs. 4 and 5, respectively.

In addition to the trapping rates, the trapping model also gives a number for the shortest lifetime (a reduced bulk lifetime) [10]. If the model is fully consistent with the measured data, this calculated lifetime will agree with the measured τ_1. In the present data this is only the case for temperatures above ~400°C (Cu) and above ~300°C (Fe). Below these temperatures the measured τ_1 falls above the calculated values. This suggests that trapping also takes place into an additional type of defects with an unresolved lifetime shorter than τ_2. It also means that the estimated values at the lower annealing temperatures (Figs. 4 and 5) are lower limits for the true trapping rates. However, the ratio of the estimated values is almost correct.

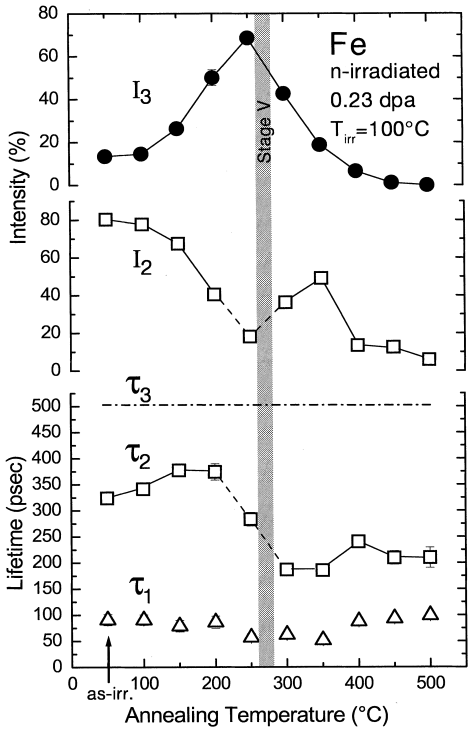

Fig. 3. The three positron lifetimes and the intensities of the two long-lived components ($I_1 + I_2 + I_3 = 100\%$) extracted from the spectra for the neutron irradiated Fe as functions of annealing temperature. The longest lifetime, τ_3, was fixed at 502 ps in the spectrum analysis. The shaded band indicates the temperature of the recovery stage V. Some of the error bars are smaller than the sizes of the data point symbols and have therefore not been shown.

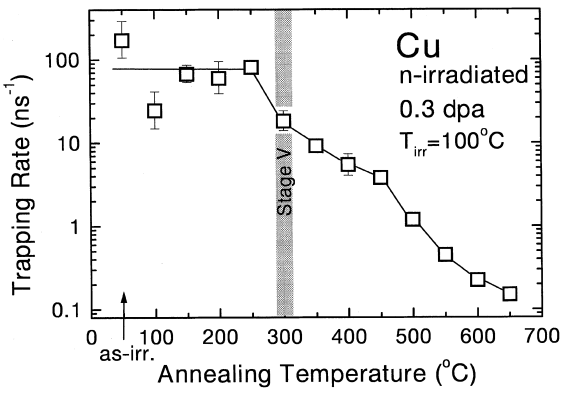

Fig. 4. The positron trapping rate into defects in the neutron irradiated Cu as a function of annealing temperature. The indicated error bars are based on the statistical scatter of the data points in the lifetime spectra. At temperatures below ~450°C the plotted points represent lower limits to the actual trapping rates. The shaded band indicates the temperature of the recovery stage V.

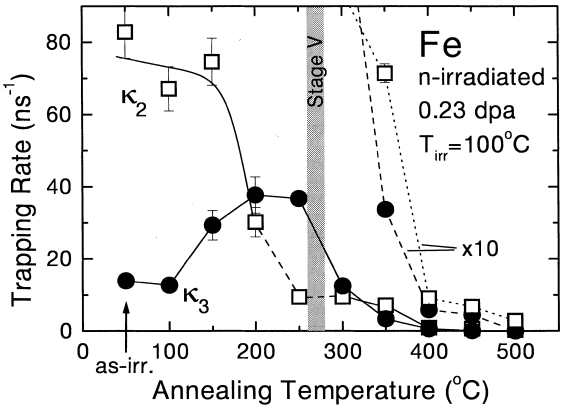

Fig. 5. The positron trapping rates into defects in the neutron irradiated Fe as functions of annealing temperature. The black circles are for trapping into voids ($\tau_3 = 502$ ps) and the open squares into micro-voids (at lower temperatures) or small clusters (at higher temperatures). The indicated error bars are based on the statistical scatter of the data points in the lifetime spectra. At temperatures below ~350°C the plotted points represent lower limits to the actual trapping rates, but the ratio of the rates (κ_3/κ_2) is approximately correct. The shaded band indicates the temperature of the recovery stage V.

As a good approximation, trapping rates can normally be assumed to be proportional to the concentrations of the defects, i.e.

$$\kappa_i = \mu_i \times C_i, \tag{1}$$

where κ_i is the trapping rate into the defects of type 'i' and C_i their density. The so-called specific trapping rate, μ_i, depends on the type of the defect. For voids, for example, μ_{void} increases with void size [10].

The results of the electrical conductivity measurements are shown in Fig. 6. Clearly, the irradiation reduces the conductivity by about 10% for both materials due to the formation of defects and transmutation products [30]. Although less detailed, the recovery of the irradiation-induced defects in the two metals on annealing is seen to take place in the same temperature regions as observed by PAS. Because of the transmutation-produced impurities the conductivities do not reach 100%, even at the highest temperatures.

5. Discussion

In general, the quantitative results (Figs. 2–5) confirm the big difference in the accumulated damage and the damage recovery between the two metals illustrated in Fig. 1. In Fe voids are formed which is not the case in Cu. Details of these results and their implications are discussed in the following.

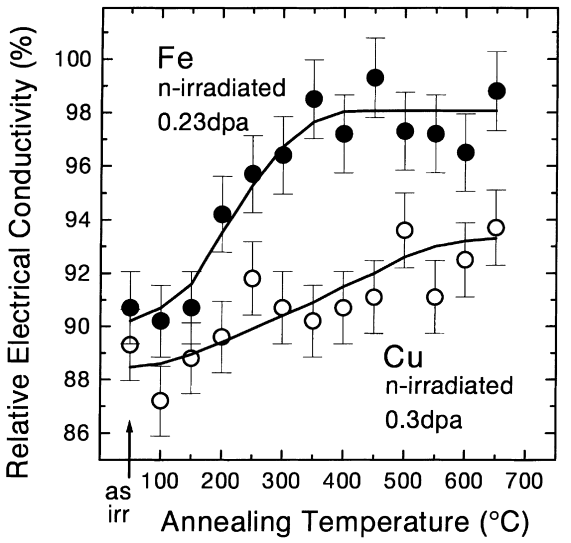

Fig. 6. Electrical conductivity as a function of annealing temperature for irradiated Fe and Cu. The plot shows the conductivities relative to those for unirradiated Fe and Cu, respectively. The recovery of the irradiation-induced defects on annealing is reflected in the conductivity increase for both metals. Because of the transmutation produced impurities, the conductivities do not reach 100% even at the highest annealing temperatures.

5.1. Copper

As seen in Fig. 2 the longest lifetime for Cu stays constant up to about 400°C (182 ps on an average) while its intensity remains constant, almost 100%, up to ~250°C but decreases at higher temperatures. The lifetime is in good agreement with the ones found earlier after deformation or neutron irradiation at lower temperatures [12] and has been ascribed to positrons trapped at small vacancy clusters or at SFT [12–15,19]. TEM shows that in the as-irradiated state the copper specimen contains a population of SFT with an average size of 2.5 nm and a density of 4.1×10^{23} m^{-3}. After an annealing of 50 h at 300°C the average size increased to 3.8 nm and the density decreased to 2.5×10^{23} m^{-3} [33]. Thus, some coarsening of the SFT population takes place, but the density of SFTs does not change appreciably by this annealing treatment.

In contrast to this, at 300°C and above (i.e. in and above stage V, 275–325°C [34]) the intensity of the 182 ps component, and hence the trapping rate (Figs. 2 and 4) decreases, in agreement with earlier findings [12]. This shows that a strong decrease in defect density takes place above 250°C. The trapping rate has apparently decreased by a factor of 4–5 at 300°C (Fig. 4). In spite of the uncertainties in the determination of trapping rates at the lower temperatures mentioned above, it seems that the SFT cannot alone be responsible for the 182 ps lifetime component. This indicates, as was already suggested in [12], that a population of small, submicroscopic vacancy clusters, probably stabilized by gas atoms or other impurities, are the main defects that trap positrons with a lifetime of 182 ps. For such vacancy clusters to be the main trapping sites, their density has to be appreciably higher than that of the SFTs. A more detailed TEM study of the annealing behaviour for comparison with the PAS results is planned.

It is interesting that the short lifetime τ_1 remains almost constant at ~100 ps in the whole temperature range, irrespective of its intensity ($I_1 + I_2 = 100\%$). This component was not observed in the similar annealing study of Cu which was neutron irradiated to a dose of 5×10^{22} n/m^2 [12], i.e. 30 times lower than that in the present work. We suggest that transmutation-produced impurities might be responsible for this lifetime component. As seen in Fig. 6 the electrical conductivity does not recover fully to 100% even at the highest temperatures. This effect is ascribed to scattering of conduction electrons on impurities produced by the irradiation [30]. Probably some of these impurities act as shallow traps for positrons. Since shallowly trapped positrons have lifetimes close to the bulk lifetime (i.e. roughly 100 ps) and since the density of impurities is about 30 times higher than in our earlier work [12] this would explain the appearance now of the ~100 ps component. The intensity of this component would have been below the detection limit in the earlier, low dose specimen.

At 450°C and above, the longest lifetime τ_2 increases to about 350 ps (Fig. 2) which is characteristic for small three-dimensional vacancy agglomerates, i.e. cavities such as small voids (~10–15 vacancies) or gas bubbles [16]. In the same temperature range the intensity (and thus the trapping rate) of this component drops rapidly. The specific trapping rate for cavities of this size is $\sim 8 \times 10^{15}$–12×10^{15} s^{-1} [10]. With the trapping rates from Fig. 4 we estimate that the density of the cavities decreases from $\sim 3 \times 10^{21}$ m^{-3} to $\sim 1.5 \times 10^{21}$ m^{-3} in the temperature range 550–650°C. The question of course arises as to what stabilises such small cavities at these temperatures. If we take the He generation rate in copper during neutron irradiation to be ~0.1–0.3 appm/dpa [35,36], the total concentration of He produced in the copper specimens is likely to be 2.5×10^{21}–7.5×10^{21} m^{-3}, i.e. roughly 1–5 He atom per cavity or an average helium density in each cavity of $n_{He} = 0.7 \times 10^{28}$–$2.5 \times 10^{28}$ m^{-3}. This is roughly 4–15 times lower density than required to maintain equilibrium He bubbles containing 10–15 vacancies (assuming the equilibrium bubble radius $R_{eq} = 2\gamma/P$, where P is the pressure that can be estimated from n_{He} via the equation of state [37]). Thus, even considering the rather large uncertainties associated with some of the quantities used in this estimate, we must conclude that the amount of

He produced by transmutation during neutron irradiation is too small to be able to stabilise the observed population of cavities at temperatures in the range 550–650°C. Maybe the hydrogen (in the form of hydrogen or hydrocarbon molecules) which is produced simultaneously with the He in quantities probably several times higher or other gaseous impurities (e.g. nitrogen) could contribute to the stabilisation of the cavities. In addition, the surface energy, γ, and hence the equilibrium bubble radius for a given gas pressure, might be influenced by impurities segregated at the cavities during annealing.

5.2. Iron

In the as-irradiated state and at the lowest annealing temperatures ($T \leqslant 100$°C) the two dominating (i.e. most intense) lifetime components are the two long-lived ones, with the lifetime values of $\tau_2 \sim 325$–375 ps and $\tau_3 = 502$ ps (Fig. 3). Both of these components must be ascribed to three-dimensional vacancy agglomerates, i.e. voids, but of different sizes. The shorter lifetime, $\tau_2 \sim 325$–375 ps, is equivalent to an average cavity sizes of ~9–14 vacancies [17]. In the following, we shall refer to these small cavities as micro-voids. The longer lifetime of ~500 ps must be associated with voids that contain (on an average) ~40–50 vacancies or more, as mentioned above. Although we ascribe the two lifetimes to two specific average void sizes, it should be pointed out that this probably represents a two-bin approximation of one wide size distribution of voids rather than two discrete void size distributions.

The trapping rate, κ_2, for the micro-voids is determined to be $\geqslant \sim 70$ ns^{-1} (Fig. 5). Taking the specific trapping rate for a void size of ~10 vacancies from [10], we obtain from Eq. (1) a density of micro-voids, $C_{\text{m-v}} >\sim 1 \times 10^{24}$ m^{-3}. The trapping rate into the larger voids, κ_3 is found to be $\geqslant 15$ ns^{-1} (Fig. 5). Assuming that the voids contain (on an average) about 50 vacancies (~1 nm in diameter) a void density of $C_{\text{v}} >\sim 1.3 \times 10^{23}$ m^{-3} is obtained from Eq. (1). If the voids are bigger than assumed, their density will be lower than this estimate. The total density of micro-voids and voids is about the same or somewhat higher than observed by TEM in Mo that had been neutron irradiated to about the same dose and at the same homologous temperature as in the present work [2,38]. It should be noted, however, that in TEM the voids are visible in Mo but not in Fe.

The recovery of the microstructure in the irradiated Fe during annealing is reflected in the changes of the PAS parameters in different temperature ranges as discussed in the following.

In the annealing temperature range of $100\text{°C} < T < 200$–250°C, κ_3 increases about three times (Fig. 5) which suggests that the density and/or the size of the voids increase significantly. Simultaneously, κ_2 and therefore the micro-void density $C_{\text{m-v}}$ decreases drastically while the increase of τ_2 (up to 200°C, Fig. 3) indicates an increase in the average micro-void size from about 10 to 15 vacancies. Thus, we are seeing an increase in the number density of voids at the expense of the micro-voids in this temperature range. Clearly, this strong coarsening of the micro-void population cannot be rationalized in terms of Ostwald ripening since the coarsening occurs at temperatures well below the recovery stage V (250–280°C [34]) where vacancies cannot evaporate from the micro-voids or voids. Hence it seems that the observed disappearance of micro-voids must happen by their migration (by a Brownian-like motion, controlled by surface diffusion of vacancies in the micro-voids [39–41]) and coalescence with other voids and micro-voids.

In the annealing temperature range of 200–300°C τ_2 decreases drastically to about 200 ps (Fig. 3). This indicates that the micro-void component disappears in this temperature range. The defects that give rise to this lifetime (i.e. ~200 ps) could be, like in Cu, very small, gas or impurity stabilised, vacancy clusters containing only a few vacancies. The trapping rate into these defects is much smaller than into the micro-voids at lower temperature (Fig. 5). Hence, these defects may have been present also below 250°C, but it has not been possible to resolve them in the lifetime spectra. To indicate that the type of defects that give rise to the τ_2 component changes in the temperature range from 200°C to 300°C, the lines that connect the points for τ_2 and I_2 in Fig. 3 and κ_2 in Fig. 5 have been dashed in this interval.

In the temperature range 250–350°C, i.e. in and above the annealing stage V, the trapping rate for voids κ_3 decreases by a factor of more than 10 (Fig. 5). This shows that the void density decreases (see Eq. (1)), either because a coarsening of the void population takes place, the voids shrink and disappear by the emission of vacancies or a combination of both (Ostwald ripening). It is interesting that the disappearance of the voids happens so close to stage V. In bcc Mo where stage V is ascribed to the disappearance of vacancy loops the voids are stable well above stage V [25,42].

The trapping rate κ_2 is roughly constant (~8 ns^{-1}) in the temperature interval 250–350°C (Fig. 5). If we accept the suggestion made above, i.e. that the defects which give rise to the τ_2, I_2 component in this temperature range are small, gas (or otherwise) stabilised vacancy clusters, we can estimate the density of these clusters to be roughly 5×10^{23} m^{-3}. A helium production rate of 0.24 appm/dpa [43] gives rise to a He concentration of $\sim 0.5 \times 10^{22}$ m^{-3}. This is much smaller than the cluster density. Hence, like for Cu, the He produced by transmutation cannot alone account for the stabilisation of these cavities. Hydrogen is produced in only about three times higher quantities than He [43]. Therefore its

contribution to the stabilisation of the population of small cavities will also be limited. So, like for copper, we are led to suggest that other (gaseous) impurities may stabilise small vacancy clusters at temperatures up to about 350°C. Above this temperature, κ_2 decreases about 10 times to a low level at 400–450°C (equivalent to a cluster density of $\sim 5 \times 10^{22}$ m^{-3}), and the defect densities reach the detection limit at ~500°C.

5.3. Comparison of defect accumulation behaviour in copper and iron

The main finding of the present work is that there is a substantial difference in the defect accumulation behaviour between fcc copper and bcc iron during neutron irradiation at 100°C, i.e. at a temperature between the annealing stages III and V. Partly as a consequence of this, also the annealing behaviour of the defect structure in these two metals is very different:

- In iron, the defect structure in the as-irradiated state is dominated by micro-voids and voids while in copper there is no indication of the presence of such three-dimensional vacancy agglomerates in the as-irradiated state. It is argued that in copper, high densities of sessile interstitial loops and stacking fault tetrahedra act as efficient sinks for vacancies and thereby prevent the evolution of a significant level of vacancy supersaturation. Such a supersaturation would be a necessary condition for the development of a void population. In iron, on the other hand where no SFT are formed and a large fraction of the glissile interstitial loops are lost at sinks such as dislocations and grain boundaries, the accumulated sink density for vacancies is much smaller [9]. These conditions are likely to cause a build-up of a vacancy supersaturation necessary for the formation and growth of voids in iron.
- On annealing, the micro-void/void population in iron coarsens significantly well below stage V. This is interpreted to occur via a Brownian-like motion of the micro-voids and voids.
- In copper in the as-irradiated state, apart from the high density of SFTs observed by TEM, it is possible that a population of very small vacancy clusters, stabilised by gases or other impurities, may be present. On annealing, there is no detectable change in defect structure below stage V (in particular no indication of cavity formation).
- On annealing through stage V and above, the void density in iron decreases rapidly and completely anneals out at ~500°C. Similarly, in copper the density of the very small, stabilised clusters shows a fast decrease on annealing through stage V.
- At the highest annealing temperatures small bubbles are formed in copper, while in iron a population of very small, stabilised vacancy clusters are revealed. In both cases, densities decrease with increasing annealing temperature.

6. Conclusions

The present work demonstrates convincingly that positron annihilation spectroscopy can provide valuable information about the microstructure of irradiated metals, in particular about the behaviour of submicroscopic voids.The obtained results and their analysis clearly show that the potential for void formation during neutron irradiation at temperatures below stage V is substantially higher in iron than in copper.

It is pointed out that this difference seems to emanate directly from the difference in the intracascade clustering of self-interstitial atoms and vacancies and from the differences in the properties of these primary clusters between bcc iron and fcc copper.

The population of micro-voids and voids in iron is found to coarsen significantly at annealing temperatures well below stage V. This is thought to occur via a surface diffusion-controlled Brownian-like motion of micro-voids and voids, and would suggest that the migration and coalescence of void embryos may be an important element in the process of void nucleation.

Acknowledgements

The present work was partly funded by the European Fusion Technology Programme. We wish to thank J.H. Evans and S. Linderoth for discussions and B. Olsen and N.J. Pedersen for technical assistance.

References

[1] B.N. Singh, J.H. Evans, J. Nucl. Mater. 226 (1995) 277.
[2] S.I. Golubov, B.N. Singh, H. Trinkaus, these Proceedings, p. 78.
[3] M.L. Jenkins, M.A. Kirk, W.J. Phythian, J. Nucl. Mater. 205 (1993) 16.
[4] W. Jäger, J. Microsc. Spectrosc. Electron 6 (1981) 437.
[5] H. Franz, G. Wallner, J. Peisl, Radiat. Eff. Def. Solids 128 (1994) 189.
[6] W.J. Phythian, R.E. Stoller, A.J.E. Foreman, A.F. Calder, D.J. Bacon, J. Nucl. Mater. 223 (1995) 245.
[7] Y.N. Osetsky, A. Serra, V. Priego, B.N. Singh, S.I. Golubov, Philos. Mag. A, in press.
[8] Yu.N. Osetsky, D.J. Bacon, A. Serra, B.N. Singh, S.I. Golubov, these Proceedings, p. 65.
[9] B.N. Singh, A. Horsewell, P. Toft, J. Nucl. Mater. 271&272 (1999) 97.
[10] M. Eldrup, B.N. Singh, J. Nucl. Mater. 251 (1997) 132.
[11] M. Eldrup, J. Phys. (Paris) IV Colloq. 5 (1995) C1-93.

[12] M. Eldrup, J.H. Evans, O.E. Mogensen, B.N. Singh, Radiat. Effects 54 (1981) 65.
[13] Y. Kamimura, T. Tsutsumi, E. Kuramoto, Phys. Rev. B 52 (1995) 879.
[14] E. Kuramoto, H. Abe, M. Takenaka, F. Hori, Y. Kamimura, M. Kimura, K. Ueno, J. Nucl. Mater. 239 (1996) 54.
[15] K. Ueno, M. Ohmura, M. Kimura, Y. Kamimura, M. Takenaka, T. Tsutsumi, K. Ohsawa, H. Abe, E. Kuramoto, Mater. Sci. Forum 255–257 (1997) 430.
[16] K.O. Jensen, R.M. Nieminen, Phys. Rev. B 36 (1987) 8219.
[17] M. Puska, R.M. Nieminen, J. Phys. F 13 (1983) 333.
[18] M. Eldrup, Mater. Sci. Forum 105–110 (1992) 229.
[19] H. Häkkinen, S. Mäkinen, M. Manninen, Phys. Rev. B 41 (1990) 12441.
[20] K. Hinode, S. Tanigawa, M. Doyama, Radiat. Eff. 32 (1977) 73.
[21] S. Mantl, W. Triftshäuser, Phys. Rev. B 17 (1978) 1645.
[22] A. Vehanen, P. Hautojärvi, J. Johansson, J. Yli-Kauppila, P. Moser, Phys. Rev. B 25 (1982) 762.
[23] P. Hautojärvi, L. Pöllänen, A. Vehanen, J. Yli-Kauppila, J. Nucl. Mater. 114 (1983) 250.
[24] K. Petersen, N. Thrane, R.M.J. Cotterill, Philos. Mag. 29 (1974) 9.
[25] M. Eldrup, O.E. Mogensen, J.H. Evans, J. Phys. F 6 (1976) 499.
[26] H.E. Hansen, H. Rajainmäki, R.M. Nieminen, Positron Annihilation, in: P.C. Jain, R.M. Singru, K.P. Gopinathan (Eds.), World Scientific, Singapore, 1985, p. 515.
[27] H. Rajainmäki, S. Linderoth, H.E. Hansen, R.M. Nieminen, J. Phys. F 18 (1988) 1109.
[28] H. Rajainmäki, S. Linderoth, J. Phys.: Condens. Matter 2 (1990) 6623.
[29] B.N. Singh, D.J. Edwards, M. Eldrup, P. Toft, Risø Report, Risø-R-937 (EN), January 1997.
[30] M. Eldrup, B.N. Singh, J. Nucl. Mater. 258–263 (1998) 1022.
[31] L. Van Hoorebeke, A. Fabry, E. van Walle, J. Van de Velde, D. Segers, L. Dorikens-Vanpraet, Nucl. Instrum. and Meth. A 371 (1996) 566.
[32] P. Kirkegaard, N.J. Pedersen, M. Eldrup, Risø Report, Risø-M-2740, 1989.
[33] B.N. Singh, D.J. Edwards, M. Eldrup, J. Nucl. Mater., unpublished.
[34] H. Schultz, P. Ehrhart, in: H. Ullmaier (Ed.), Atomic Defects in Metals, Landolt-Börnstein, New Series, vol. 25, Springer, Berlin.
[35] H.R. Brager, H.L. Heinisch, F.A. Garner, J. Nucl. Mater. 133&134 (1985) 676.
[36] H.R. Brager, J. Nucl. Mater. 141–143 (1986) 79.
[37] S.E. Donnelly, Radiat. Eff. 90 (1985) 1.
[38] J. Bentley, B.L. Eyre, M.H. Loretto, in: M.T. Robinson, F.W. Young, Jr. (Eds.),Fundamental Aspects of Radiation Damage in Metals, US-ERDA Conf.-751006, 1975, p. 925.
[39] P.J. Goodhew, S.K. Tyler, Proc. Roy. Soc. London A 377 (1981) 151.
[40] S.E. Donnelly, J. H. Evans (Eds.), Fundamental Aspects of Inert Gases in Solids, Plenum, New York, 1991.
[41] B.N. Singh, A.J.E. Foreman, in: R.S. Nelson (Ed.), Consultant Symposium; The Physics of Irradiation Produced Voids, AERE-R7934, H.M. Stationary Office, January 1975, p. 205; Scripta Met. 9 (1975) 1135.
[42] J.H. Evans, UKAEA Report AERE-R7966, 1975.
[43] K. Ehrlich, A. Möslang, Nucl. Instrum. and Meth. B 139 (1998) 72.